Limits of the frequency response for the analysis of ripple-based controllers

Jorge Cortés,Vladimir Šviković, Pedro Alou, Jesús Oliver and Jose A. Cobos Rafael Wisniewski

I. Introduction

Designers of power converters in the industry mainly use techniques based on the frequency response to analyze these systems [1]. The linear controller of the system is designed according to the desired loop gain of the system. The stability is established by means of the gain margin and the phase margin of the corresponding Bode diagram. For a good dynamic behavior, the phase margin is set between 60° and 80° (usually 76°). The output impedance transfer function $Z_{out}(s) = -v_{out}/i_{out}$ can be used to estimate also the dynamic behavior under load steps. In general, frequency response-based techniques provide useful tools to design accurately the linear controller of the power converter.

However, the frequency response is applied to the slow loop of the system. Figure 1 shows an example of a ripple-based control. These kinds of controls are used to supply microprocessors where the converter has to meet high dynamic requirements and a very high switching frequency for integration purposes. These controls typically present two parts: an outer slow loop where the output voltage is controlled with a linear controller and an inner fast loop where a rippled signal is compared to the output of the controller to obtain the duty cycle. Figure 2 shows the experimental loop gain of the slow loop at the border of a sub-harmonic oscillation and within it, proving that the slow loop is completely "blind" to the instabilities of the fast loop. The signals of this fast loop present most of its harmonic content around the switching frequency and, since the bandwidth of the control is much lower than this frequency, a simple averaged model cannot predict some instabilities.

Unfortunately, the dynamic behavior and the appearance of sub-harmonic oscillations heavily depend on the fast loop and, therefore, an alternative analysis is required to design robust and fast converters. The prediction of sub-harmonic oscillations requires a very accurate model of the transfer functions of the fast loop. A simulation program such as *Simplis* to obtain the corresponding Bode diagrams falls short in order to derive a wide stability criteria for sensitivity analysis where several critical parameters are varied and a mathematical or graphical representation of the stability criteria is needed.

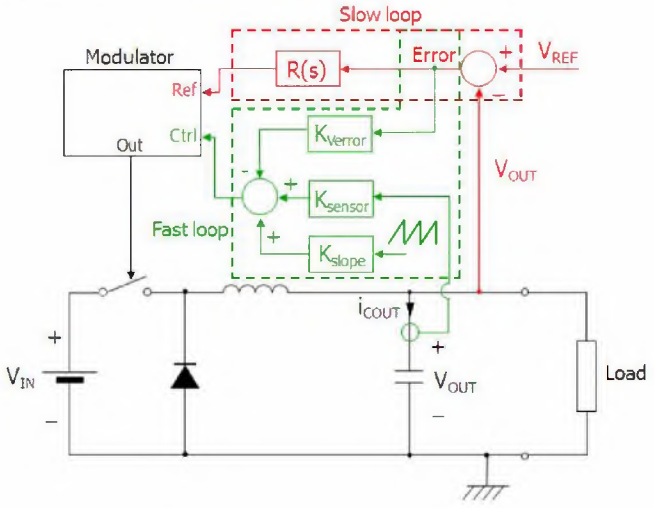

Fig. 1: V^2I_c, a ripple-based controller.

An approach to design these systems is to introduce information about the ripple of the signals in the averaged model [2], [3]. These methods, which still rely on the frequency response, are widely known by designers and obtain a non-linear PWM modulator to provide a methodology to design the compensating ramp of peak current-mode controls but the modulation block that is needed to derive may be prohibitively complex in ripple-based controllers. The descriptive function [4] is proposed to analyze a V^2 controlled-buck converter.

This work has been partially supported by Spanish Government Innovation and Science Office (MCINN), under research grant no. DPI- 2010-20096, "FAST" project.

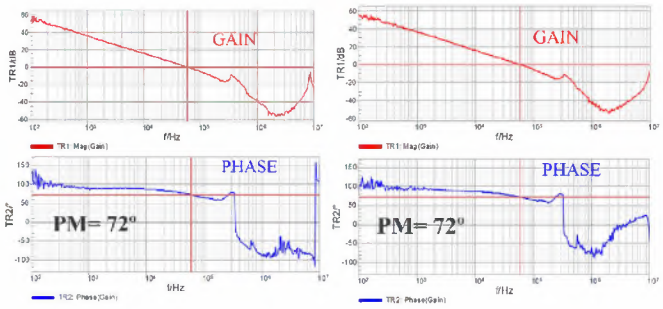

(a) (b)

Fig. 2: Experimental loop gain of the slow voltage loop in $V^2 I_c$ control before and within the instability of figure 16.

The power stage, the switches and the PWM modulator are treated as a single entity and modeled. This still relies on the matrix are all inside the unit circle. The monodromy matrix is the matrix that relates the perturbation at the beginning of a period and the perturbation at the end of that period $\triangle x(T) = \phi_{CYCLE} \cdot \triangle x(0)$.

Depending on the system, several methods to obtain the monodromy matrix are available. Periodic systems can be classified in three types: continuous systems, discrete systems and hybrid systems. The power converter as a continuous system is known in power electronics as an averaged linearized model. However, continuous systems cannot present double-period bifurcations [5] (sub-harmonic oscillations) and, thus, this kind of modeling is not suitable for a complete analysis.

A. *Monodromy matrix of discrete systems*

A discrete system [8] is of the form of $x_{k+1} = f(x_k, u)$

state dx/dt just after the switching and n is the normal to the hyper-surface $h(x(t),t)$ ($n = K$ if (3) applies).
Note that when the switching is forced (as in controls using a latch RS), the switching condition is not an actual hyper-surface[1] and, therefore, the term n of the equation (4) is a vector of zeros so the saltation matrix at that instant is the identity matrix.

For a system that starts in state 1, then at $t = t_1$, it switches to state 0 and continues in that state until it switches back at $t = t_2$ to state 0 (figure 4), the monodromy matrix is:

$$\phi_{CYCLE} = S_0(t_2) \cdot e^{A_0 \cdot (t_2 - t_1)} \cdot S_1(t_1) \cdot e^{A_1 \cdot (t_1)} \quad (5)$$

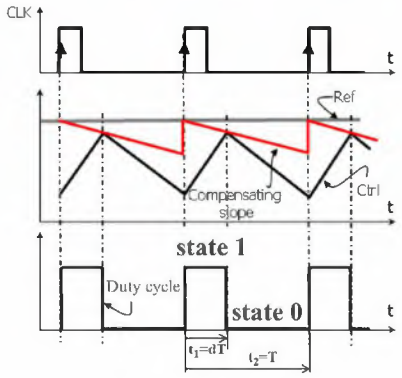

Fig. 4: Switching diagram of V^2I_c control.

III. V^2I_c CONTROL OF A BUCK CONVERTER AND ITS MATHEMATICAL MODEL

In this section, the main concepts of the V^2I_c control [11] (figure 5) are explained. The V^2I_c control is proposed for buck

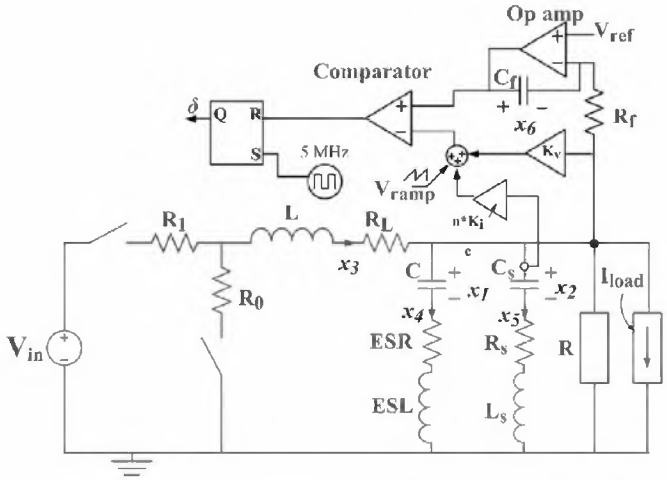

Fig. 5: Electrical scheme of a V^2I_c controlled buck converter.

converters switching at 5 MHz that supply microprocessors. It provides very fast transient responses under voltage reference steps and load steps. The control presents an inner fast loop where the current through the capacitor, the output voltage and a compensating ramp to stabilize the system are added. In the outer slow loop, the error of the output voltage passed through a linear controller. The ON-resistance of the switches R_1 and R_0, the resistance of the inductor, R_l, and the ESR, R_c, and the ESL of the output capacitor are the parasitic elements of the power stage. The output of the control is δ which is the duty cycle. The compensating ramp, V_{ramp} is modeled over a period T as $V_{ramp} = m_{ramp}t + H_f$ where m_{ramp} is the slope of the ramp and H_f is the offset. The peak-to-peak amplitude of the ramp is $V_{pp} = m_{ramp}/T$.

A. Measurement of the current through the output capacitor

The current through the output capacitor is measured by adding a parallel RLC network [12]. The actual implementation is done by means of a trans-impedance amplifier but, for the purpose of this paper, it is sufficient to consider only the equivalent parallel RLC network. For a correct measurement of the current, the parameters of the parallel network must comply the following conditions:

$$C_S = n \cdot C;\ R_S = ESR/n;\ L_S = ESL/n \quad (6)$$

When these conditions are fulfilled, the current through the parallel network is n times the current through the output capacitor

$$i_S = n \cdot i_C$$

A mismatch in the ESL of the output capacitor may induce sub-harmonic oscillations.

B. Piece-wise smooth model of the system

The state variables of the system are: the voltage in the output capacitor, x_1, the voltage in the capacitor of the parallel network, x_2, the current through the inductor, x_3, the current through the output capacitor, x_4, the current through the parallel network, x_5, and the voltage in the capacitor of the regulator, x_6.
The general form of a piece-wise smooth model is shown in (2) but, due to the integral action, the matrices A_0 and A_1 are singular. Then, the solution of the differential equation $dx(t)/dt = Ax(t) + Bu$, needed for the derivation of the discrete model, cannot be directly solved, and rather, the solution is separated between the solution of the state variables that depend on themselves $x_s = [x_1;\ x_2;\ x_3;\ x_4;\ x_5]$ and the solution of the state variable that does not depend on itself $x_c = x_6$.

The piece-wise smooth model of the system is:

$$\frac{dx(t)}{dt} = \begin{cases} \overbrace{\begin{pmatrix} A_{s0} & 0 \\ A_c & 0 \end{pmatrix}}^{A_0} \overbrace{\begin{pmatrix} x_s(t) \\ x_c(t) \end{pmatrix}}^{x(t)} + \overbrace{\begin{pmatrix} B_{s0} \\ B_c \end{pmatrix}}^{B_0} u, & \text{if } \delta \text{ is 0} \\ \overbrace{\begin{pmatrix} A_{s1} & 0 \\ A_c & 0 \end{pmatrix}}^{A_1} \overbrace{\begin{pmatrix} x_s(t) \\ x_c(t) \end{pmatrix}}^{x(t)} + \overbrace{\begin{pmatrix} B_{s1} \\ B_c \end{pmatrix}}^{B_1} u, & \text{if } \delta \text{ is 1} \end{cases} \quad (7)$$

[1] An hyper-surface must depend on the state variables and be differentiable with respect to them. In the case of a forced switching, the switching condition is time-dependent only and therefore $S = I$.

The switching hyper-surface that takes into account the switching from state 1 to state 0 is:

$$h_{10}(x,t) - K_f x_s(t) \mid K_c x_c(t) \mid G_f u \mid m_{ramp} t \mid H_f \quad (8)$$

The other switching does not need to be considered since it is forced by the latch RS. The elements of the matrices and vectors of (7) and (8) are shown in the Appendix.

C. Discrete model of the system

A discrete-time system is derived from (7) and (8). The result is shown in the Appendix and it is an implicit discrete model where the duty cycle is obtained numerically in each period. The discrete model is of the form:

$$x_{k+1} - f(x_k, u, d) \quad (9)$$
$$g(x_k, d) - 0$$

Normally, this system would be explicit, where the duty cycle can be obtained as an explicit function of the initial state, but this is achieved by simplifying the exponential terms of the equations by their first or second Taylor expansions. However, the requirement of considering the ESL of the output capacitor causes the mentioned simplification not to hold.

Note that the discrete model is *not* a discrete transfer function $G(z)$, but the complete equations that relate the final state with the initial state, meaning that it presents no simplifications and the ripple of the signals can be obtained from such model. This is the large-signal closed-loop discrete model of the system.

Figures 6 and 7 show a comparison between the discrete model derived and simulation results. The dynamic behavior, ripple of the signals and instabilities greatly agree.
Figure 8 shows a bifurcation diagram for sensitivity analysis. As a parameter of the power converter is varied, the value of one state variable at the beginning of each period is plotted a large number of times when the steady state has been reached. This way, a graphical representation of the bifurcation phenomena is achieved. Note that the instability, called in power converters sub-harmonic oscillation, is a double-period bifurcation where the system is unable to achieve periodicity in a period T and, rather, the equilibrium point is $2T$-periodic.

D. Comparison with averaging

The discrete model (9) depends solely on the elements of piece-wise smooth model (7) and how the switching takes place (8). Although at a first glance, the equations of the discrete model are intimidating, they are the very same equations for a vast quantity of power stages and control since the only thing that changes are the (A_i, B_i, K_f,...) matrices and vectors, which are easily known. To derive the model of another control and to consider parasitic elements is very simple. The bifurcation diagrams obtained from the discrete model can be used for sensitivity analysis.

Oppositely, in the averaged model, if considering parasitic elements is a requirement (as for sensitivity analysis) prohibitive complex different equations may need to be derived

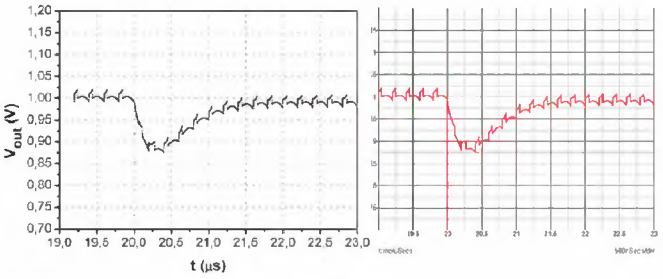

(a) Output voltage

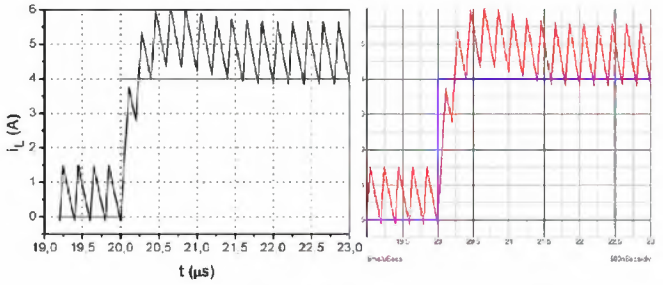

(b) Inductor current

Fig. 6: Comparison between the discrete model (left) and simulation results (right) under a load step $0A \rightarrow 4A$.

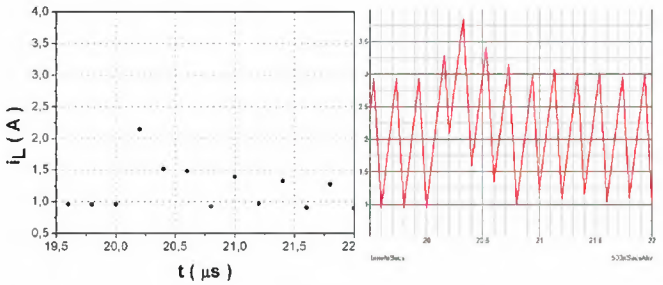

Fig. 7: Inductor current. Comparison between the discrete model (left) and simulation results (right). A mismatch in the parallel network causes a sub-harmonic oscillation at $V_{out} = 3.1V$ in both cases. Only the values of the inductor current at the beginning of each period are shown in the discrete model.

for every particular power converter. Also, the averaging and linearization of the system that are required eliminate information about the system near the switching frequency.

The discrete modeling is a vastly superior technique than the averaged modeling. However, techniques based on the frequency response, that is the common analysis, cannot be employed in the discrete model, but the next chapters show that the Floquet theory, which can be applied, is also a superior technique in ripple-based controllers.

IV. Stability analysis of $V^2 I_c$

This chapter shows the stability analysis of the $V^2 I_c$ control using the Floquet theory. The Filippov's method is employed to find out the monodromy matrix. Figure 3 shows that the piece-wise model and the value of the state variables in steady state at the switching events are needed.

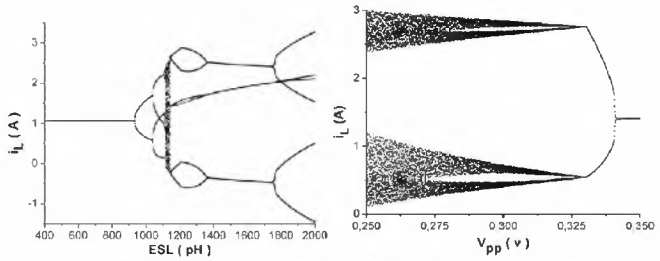

(a) Varying ESL. Sub-harmonic oscil-(b) Varying V_{pp} of comp. ramp. Sub-
lation at ESL $> 930pH$. harmonic oscillation at $V_{pp} < 0.34V$.

Fig. 8: Bifurcation diagrams for sensitivity analysis varying ESL of C_{out} and compensating ramp. Sensor designed for $ESL_n = 444pH$.

A. Values of the state variables

The required values can be retrieved from a simulation program, but, the derivation of the discrete model offers another method. From equation 9, the constraint $x_{k+1} = x_k$ is applied. Then, the values of the state variables in steady state at the beginning of the period are found out numerically (shown in the Appendix). The very same equation 9 allows then to find out the values of the state variables at the switching events. The equations are shown in the Appendix. In V^2I_c control, the latch RS forces a switching every T seconds, so that event does not have to be considered. Only, the values of the state variables at the first switching event $x(dT)$ are retrieved.

B. Filippov's method

The equation 5 shows the expression of the monodromy matrix using the Filippov's method. The saltation matrix corresponding to the second switching is the identity matrix as the switching is forced. The saltation matrix corresponding to the first switching, that occurs at $t = dT$ is:

$$S_1(dT) = I + \frac{(f_{dT+} - f_{dT-})n^T}{n^T f_{dT-} + \dfrac{\partial h}{\partial t}(dT, x(dT))}$$

where $f_{dT+} = A_0 x(dT) + B_0 u$, $f_{dT-} = A_1 x(dT) + B_1 u$ and (8) $n = [K_f,\ K_c]$, $\partial h/\partial t(dT, x(dT)) = m_{ramp}$.

The monodromy matrix is:

$$\phi_{CYCLE} = e^{A_0(1-d)T} \cdot S_1(dT) \cdot e^{A_1 dT}.$$

If all the eigenvalues are in the open unit disk, the system is locally asymptotically stable.

Figure 9 is a comparison between the bifurcation diagram of figure 8.a and the stability analysis showing a complete agreement.

V. Sensitivity analysis of ripple-based controllers

The combination of discrete modeling and Floquet theory allows the derivation of powerful tools. As critical parameters of the power converter are varied, the required values of the state variables are retrieved from the discrete modeling and the Filippov's method is employed to find out the Floquet multipliers and establish stable region diagrams. The method

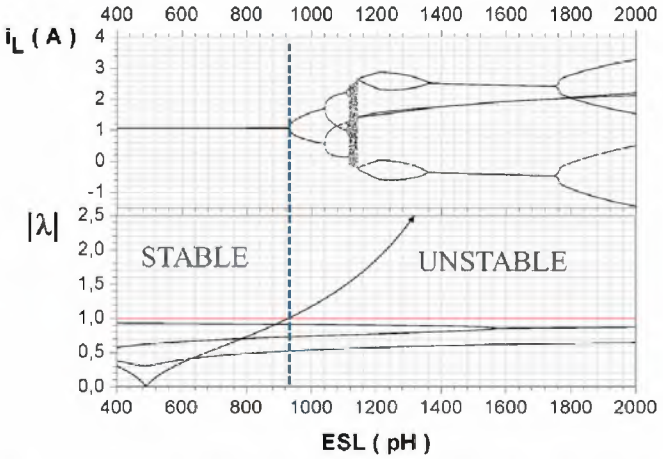

Fig. 9: Comparison the bifurcation diagram of figure 8.a and the stability analysis. When the module of one eigenvalue surpasses the unity, a bifurcation appears in the discrete model. Sensor designed for $ESL_n = 444pH$.

is applied to a buck converter with V^2I_c control [4], V^2 constant T_{on} [13] and V_{out} hysteresis with measurement of I_{Cout} (figure 10).

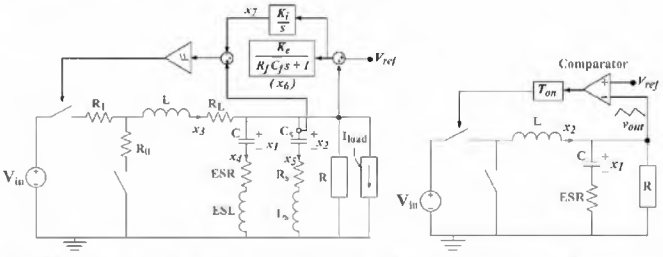

(a) V_{out} hysteresis with measurement of I_{Cout} (b) Open-loop V^2 current mode with constant T_{on}

Fig. 10: Two different types of ripple-based controllers.

A. Sensitivity analysis of V^2I_c

V^2I_c presents sub-harmonic oscillations for duty cycles greater than 0.5. A mismatch in the ESL of the output capacitor causes sub-harmonic oscillations. Also, the gain of the current loop affects the stability. A compensating ramp is added to stabilize the system. The design should consider then, what the required compensating ramp is for different duty cycles, gains of the current loop and mismatches in the parallel network. Figure 11 shows the sensitivity analysis by means of stable region diagrams.

B. Sensitivity analysis of V^2 constant T_{on}

V^2 control uses the ripple of the output voltage when the ESR of C_{out} dominant. When the switching frequency or the ESR are too low, a sub-harmonic oscillation may appear. Using a refined averaged model called descriptive function, where the information of the ripple is included in the modulation block, the following condition for stability is achieved:

$$\text{Stable when } \frac{T_{on}}{2} < ESR \cdot C_{out}$$

Figure 12 shows the sensitivity analysis using the descriptive function and the Floquet theory. The descriptive function is

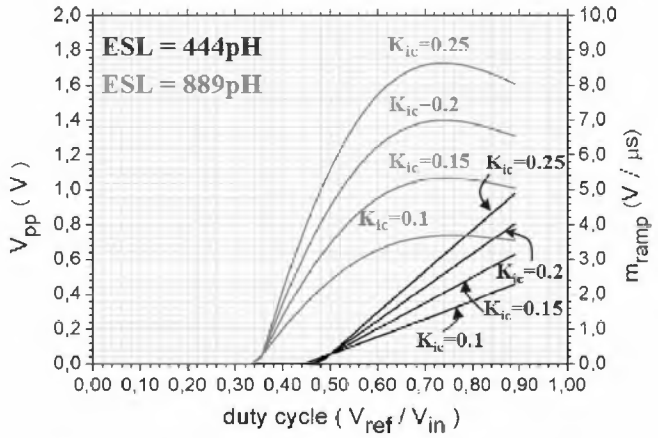

Fig. 11: Sensitivity analysis of $V^2 I_c$. It shows the required compensating ramp for different duty cycles. ESL and gain of the current loop. The stable regions are the upper area of the proper curve, see figure 15 for reference. Sensor designed for $ESL_n = 444pH$.

more conservative and the Floquet theory is more accurate and allows for a smaller capacitor or lower switching frequency.

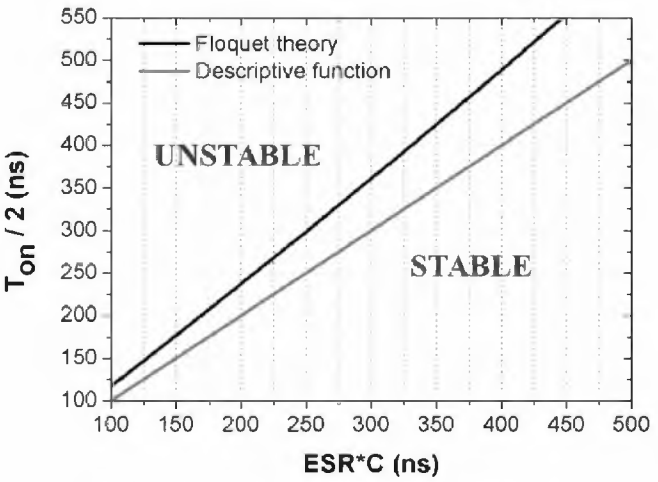

Fig. 12: Sensitivity analysis of V^2 constant T_{on}.

C. Sensitivity analysis of V_{out} with measurement of I_{Cout}

V_{out} with measurement of I_{Cout} presents the same problems as $V^2 I_c$ under a mismatch in the parallel network. Figure 13 shows the sensitivity analysis varying the ESL of C_{out} and the duty cycle. As the region of instability is too small, the figure shows the evolution of the modules of the Floquet multipliers.

VI. Experimental results

This section documents the validation of the discrete modeling and stability analysis of the $V^2 I_c$ control. The experimental prototype is designed according to the sensitivity analysis of the section V.

The experimental system switches at a frequency of $5\ MHz$. The input voltage V_{in} is $4.5V$ and the nominal output voltage V_{out} is $1V$. The parameters of the power stage are: $R_1 = R_0 = 40m\Omega$, $L = 100nH$, $R_L = 10m\Omega$, $C = 4\mu F$, $ESR = 4.86m\Omega$, $ESL = 1.2nH$. For a well-designed sensor:

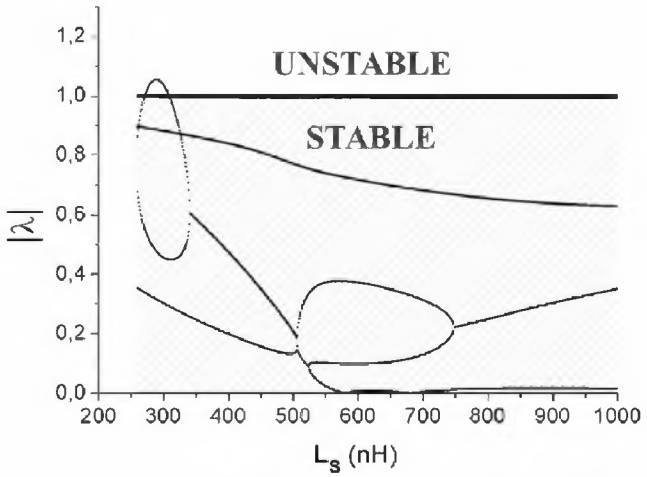

Fig. 13: Sensitivity analysis of V_{out} with measurement of I_{Cout}. The sub-harmonic oscillation appears in a small region between $L_s = 250nH$ and $310nH$. Sensor designed for $L_S = 444nH$.

$C_S = 4nF$, $R_S = 4.86\Omega$, $L_S = 1.2\mu H$. The parameters of the control are: $f_{sw} = 5MHz$, $d_{min} = 5\%$, $d_{max} = 95\%$, $V_{pp} = m_{ramp}/T = 1.3V$, $K_{ic} = 0.245$, $K_v = 1$, $R_f = 1k\Omega$, $C_f = 2.42nF$.

The comparison of the discrete map and the experimental results is shown under load steps and voltage reference steps. For each case, a positive and a negative step is plotted. The section is divided in two parts where the modeling and the stability analysis are validated respectively.

A. Validation of modeling

The discrete modeling of the system is validated by comparing it the dynamic behavior of the system under voltage reference step of the experimental prototype.

1) Voltage reference step: The system is plotted under a negative voltage reference step of $2\ V \rightarrow 1\ V$ (figure 14).

The dynamic behaviors of the discrete model and the experimental prototype greatly agree.

B. Validation of analysis of local stability

The previous parameters remains the same except the ramp, which is set to an amplitude of $0.37V$ in order to induce an instability.

Employing the Filippov's method to find out the Floquet multipliers, the system is predicted to get unstable from $3.1\ V$ (figure 15).

This prediction is validated experimentally (figure 16). Note that the reference signal V_{slow}, which is the output of the linear controller, does not change, meaning that the slow loop is unaware of the oscillation in the fast loop.

VII. Conclusion

The discrete model is an extremely accurate technique. It is simpler than averaged-based method for fast control techniques, where parasitic elements are considered. The Floquet theory predicts with extreme precision sub-harmonic oscillations of the power converters. The Floquet theory along with

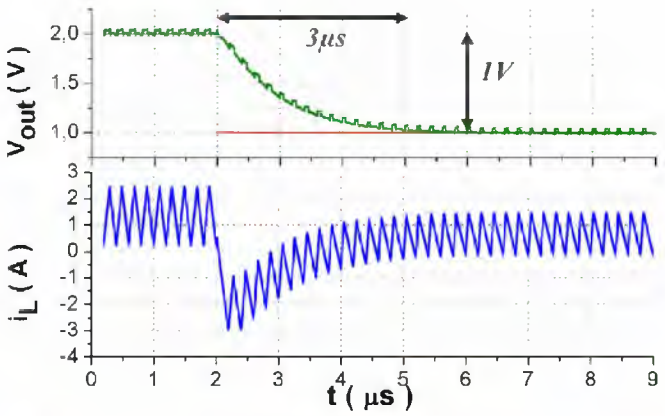

(a) Discrete model

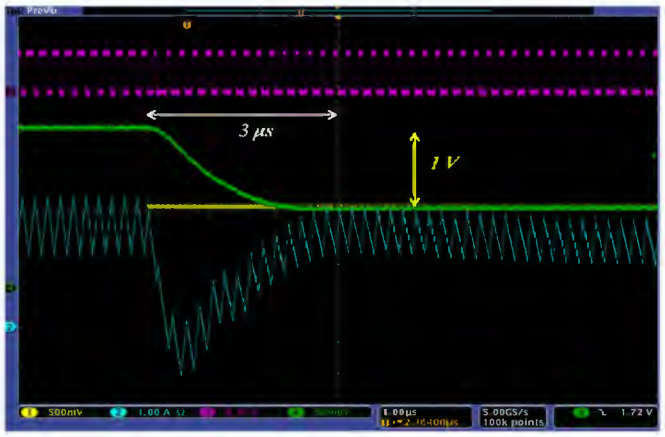

(b) Experimental results

Fig. 14: Experimental results: Negative voltage reference step of 1 V from 2 V to 1 V, output voltage in green (500 mV/div), voltage reference in yellow (500 mV/div), inductor current in blue (1 A/div), (b) measured current in purple (500 mV/div) and gate signal in purple (5 V/div) with 1$\mu s/div$ time scale.

the discrete model allows for sensitivity analysis regarding the tolerances of critical parameters.

Appendix A
Mathematical Formulas

This appendix contains all the mathematical formulas derived for the analysis.

A. Piece-wise smooth model of V^2I_c

The piece-wise smooth model of the system is:

$$\frac{dx(t)}{dt} = \begin{cases} \begin{pmatrix} A_{s0} & 0 \\ A_c & 0 \end{pmatrix} x(t) + \begin{pmatrix} B_{s0} \\ B_c \end{pmatrix} u, & \text{if } \delta \text{ is 0} \\ \begin{pmatrix} A_{s1} & 0 \\ A_c & 0 \end{pmatrix} x(t) + \begin{pmatrix} B_{s1} \\ B_c \end{pmatrix} u, & \text{if } \delta \text{ is 1} \end{cases}$$

$$x(t) = \left(x_s(t);\ x_c(t)\right)^T; \qquad u = \left(V_{in},\quad V_{ref},\quad I_{load}\right)^T$$

$$K_i = 1/R_f C_f; \quad A_c = \left(0,\quad 0,\quad -K_i R,\quad K_i R,\quad K_i R\right)$$

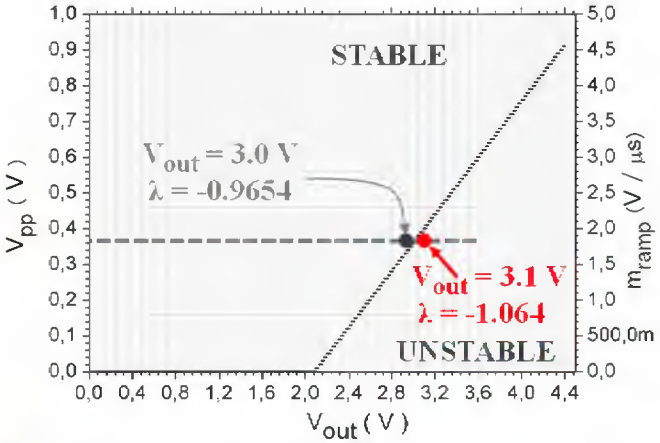

Fig. 15: Stable region diagram varying compensating ramp and output voltage. The figure shows that the system gets unstable for output voltages greater than $3V$ when V_{pp} 0.37 V. The value of the eigenvalue that goes out of the unit circle is shown.

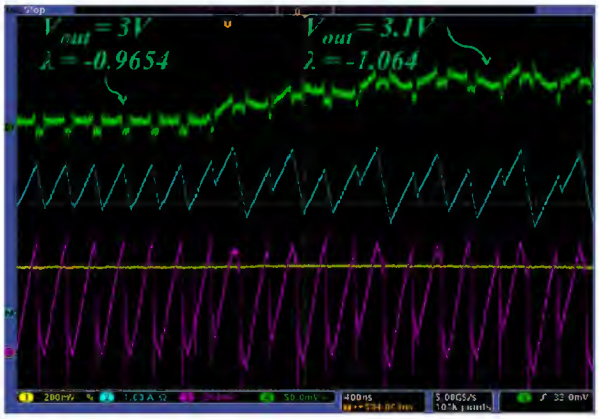

Fig. 16: Experimental results: positive voltage reference step of 0.1 V from 3 V to 3.1 V, output voltage in green (AC coupling, 50 mV/div), inductor current in blue (1 A/div), control signal V_{fast} in purple (200 mV/div) and reference signal V_{slow} in yellow (200 mV/div) with 400ns/div time scale.

$$A_{s0} = \begin{pmatrix} 0 & 0 & 0 & 1/C & 0 \\ 0 & 0 & 0 & 0 & 1/C_S \\ 0 & 0 & -(R_0+R_L-R)/L & R/L & R/L \\ -1/ESL & 0 & R/ESL & -(R-ESR)/ESL & -R/ESL \\ 0 & 1/L_S & R/L_S & R/L_S & (R \mid R_S)/L_S \end{pmatrix}$$

$$A_{s1} = \begin{pmatrix} 0 & 0 & 0 & 1/C & 0 \\ 0 & 0 & 0 & 0 & 1/C_S \\ 0 & 0 & -(R_1+R_L-R)/L & R/L & R/L \\ -1/ESL & 0 & R/ESL & -(R-ESR)/ESL & -R/ESL \\ 0 & 1/L_S & R/L_S & R/L_S & (R \mid R_S)/L_S \end{pmatrix}$$

$$B_c = \left(0,\quad K_i,\quad K_i R\right)$$

$$B_{s0} = \begin{pmatrix} 0 & 0 & 0 \\ 0 & 0 & 0 \\ 0 & 0 & R/L \\ 0 & 0 & -R/ESL \\ 0 & 0 & -R/L_S \end{pmatrix}; \qquad B_{s1} = \begin{pmatrix} 0 & 0 & 0 \\ 0 & 0 & 0 \\ 1/L & 0 & R/L \\ 0 & 0 & -R/ESL \\ 0 & 0 & -R/L_S \end{pmatrix}$$

Note that x_s is a vector of five state variables, x_c is a unique state variable. Note that if the ON-resistances of the MOSFET

transistors R_1 and R_0 are the same, then, $A_1 = A_0$. The complexity of the model is because a lot of parasitic elements are considered. In the simplest case, the model only presents two state variables.

The switching conditions at the first and second event are:

$$h_{10}(x,t) = K_f x_s(t) + K_c x_c(t) + G_f u + m_{ramp} t + H_f$$

$$h_{01}(t) - t - T$$

where

$$K_f - \left[0,\ 0,\ K_v R,\ -K_v R,\ nK_{ic} - K_v R\right]$$

$$G_f - \left[0,\ -1,\ -K_v R\right]; \qquad K_c - -1$$

B. Discrete modeling

The equations of the discrete model are intimidating but, looking deeper into them, they are very simple in the sense that it is only dependable on the piece-wise model and the switching actions. The following equations are the same for every power converter and they do not have to be derived everytime. The only thing that changes from one converter to another is the piece-wise model and switching action, both easily derived.

Defining the terms:

$$N_1(d) - e^{A_{s1} dT}; \quad N_0(d) - e^{A_{s0}(1\ \ d)T}; \tag{10}$$

$$M_1(d) - A_{s1}^{-1}[N_1(d) - I]; \quad M_0(d) - A_{s0}^{-1}[N_0(d) - I]$$

Then, the function that relates the state at $t - dT$ with the initial state is:

$$x(dT) - f_d(x(0), u)$$

$$x_s(dT) = N_1(d) x_{sk} + M_1(d) B_{s1} u \tag{11}$$

$$x_c(dT) - A_c M_1(d) x_{sk} \ | \ (A_c A_{s1}^{-1} M_1(d) B_{s1} - \ldots$$

$$\ldots - dT A_c A_{s1}^{-1} B_{s1} + dT B_c) u + x_{ck}$$

The function that relates the final state with the initial state (equation 9) is:

$$x(dT) - f(x(0), u)$$

$$x_{sk\ \ 1} = K_n(d) x_{sk} + G_n(d) u \tag{12}$$

$$x_{ck-1} - K_m(d) x_{sk} \ | \ G_m(d) u \ | \ x_{ck} \tag{13}$$

where

$$K_n(d) - N_0(d) N_1(d);$$

$$G_n(d) = N_0(d) M_1(d) B_{s1} + M_0(d) B_{s0};$$

$$K_m(d) - A_c[M_0(d) N_1(d) + M_1(d)];$$

$$G_m(d) - A_c\Big[M_0(d) M_1(d) B_{s1} + \ldots$$

$$\ldots + A_{s0}^{\ 1} M_0(d) B_{s0} + A_{s1}^{\ 1} M_1(d) B_{s1}\Big] + \ldots$$

$$\ldots + (B_c - A_c A_{s0}^{-1} B_{s0})(1-d)T + (B_c - A_c A_{s1}^{-1} B_{s1}) dT$$

The function that relates the duty cycle with the initial state ((equation 9) is:

$$g(x(0), d) - 0$$

$$g(x_k, d) - K_h(d) x_{sk} + K_c x_{ck} + G_h(d) u + m_{ramp} dT + H_f - 0 \tag{14}$$

where

$$K_h(d) = K_f N_1(d) + K_c A_c M_1(d)$$

$$G_h(d) - K_f M_1(d) B_{s1} + G_f + K_c(A_c A_{s1}^{-1} M_1(d) B_{s1} - \ldots$$

$$\ldots - A_c A_{s1}^{\ 1} B_{s1} dT + B_c dT)$$

C. Equilibrium point

If the discrete model is constrained to fulfill the condition $x_{k+1} - x_k$, the expression of the equilibrium point of the system is reached:

$$0 - [K_m(d)(I - K_n(d))^{-1} G_n(d) + G_m(d)] u \tag{15}$$

$$x_{sk} - [I - K_n(d)]^{-1} G_n(d) u$$

$$x_{ck} - \frac{-1}{K_c}(K_h(d) x_{sk} \ | \ G_h(d) u \ | \ m_{ramp} dT \ | \ H_f)$$